ELSEVIER

Experimental investigation of two-stream mixing flows with streamwise and normal vorticity

S. C. M. Yu and T. H. Yip
Thermal and Fluids Engineering Division, School of Mechanical and Production Engineering, Nanyang Technological University, Singapore

This study provides detailed velocity information in the mixing region of two-stream mixing flows wit h streamwise and normal vorticity for the computational fluid dynamics (CFD) methods validation. Three trailing-edge configurations for the dividing mechanism had been considered; namely, a convoluted plate, a lobed forced mixer, and a scalloped forced mixer. The first two have been examined previously by visualization tests (Manning 1991). A velocity ratio of 0.6 was generated with initial turbulent boundary layers and was nominally two-dimensional (2-D). Velocity measurements were made on fine cross-plane grids across the wake region and at several streamwise locations using a two-component laser-Doppler anemometer (LDA). The streamwise vortex development for the lobe mixer and the scalloped mixer underwent a three-step process by which it was formed, intensified, and quickly dissipated. The shear layer growth rates were rapid for the scalloped mixer and lobed mixer cases from the trailing edge to a point where the streamwise vorticity was almost dissipated. Consequently, the growth rate reduced and became lower than that of the convoluted plate. In the absence of the streamwise vorticity, the growth rate for the convoluted plate relied only on the 2-D roll-up of the normal vorticity.

Keywords: scalloped lobed forced mixer; convoluted plate; streamwise and normal vorticity

Introduction

The present work is concerned with turbulent mixing in two-stream flows with the presence of the streamwise and normal vorticity. The practical importance of these flow situations stems from their application in many engineering devices, such as industrial burners, ejectors and turbofan engine exhausts, where the turbulent mixing of two coflowing streams is often of primary importance to the efficiency of such devices.

It has been shown that streamwise vorticity enhances mixing in a two-stream mixing layer in addition to that caused by the normal vorticity originated from the Kelvin–Helmholtz instability. The natural formation for the streamwise vorticity could be found only in cases with laminar initial conditions (Bell and Mehta 1992), and some distances are normally required from the trailing edge before it can actually be developed. To provide rapid mixing, streamwise vorticity can be introduced into the coflowing streams by other means; for example, by installing vortex generators immediately upstream of the trailing edge or having a corrugated trailing-edge profile (Bell and Mehta 1993).

Splitter plates with a convoluted trailing edge are commonly referred to as "lobed forced mixers." The geometry of the lobe causes large-scale, streamwise vorticity to be shed at the trailing edge. The enhanced mixing characteristics of the lobed mixers are directly attributable to the large mixing scales generated by the streamwise vorticity (Eckerle et al. 1992; Yu et al. 1995).

When the velocity of the stream on one side of the lobed mixer differs from that on the other side, the resulting downstream wake will not only consist of streamwise vorticity associated with the three dimensionality of the mixer but also normal vorticity associated with the difference in velocities. Furthermore, the convolution of the trailing edge would also increase the interfacial area between the two streams (relative to a flat plate). Both McCormick and Bennett (1994) and Manning (1991) have shown that they were all significant contributors to the mixing enhancement of forced lobed mixers. A high normal vorticity shed at a trailing edge would certainly lead to a faster mixing rate (Manning 1991; Eckerle et al. 1992; and McCormick and Bennett 1994) and a faster decaying rate for the streamwise vorticity (Yu et al. 1996). The present study intends to complement the visualization studies of Manning by providing detailed velocity information for the computational fluid dynamics (CFD) validation, with particular reference to the wake growth rate and streamwise vorticity decay rate. Three dividing mechanisms for the two streams were used: a lobed forced mixer; a convoluted plate; a scalloped lobed forced mixer. The first two were considered by visualization tests (Manning).

Address reprint requests of Dr. S. C. M. Yu, Thermal and Fluids Engineering Division, School of Mechanical and Production Engineering, Nanyang Technological University, Singapore 639 789, Singapore.

Received 11 January 1996; accepted 6 August 1996

Int. J. Heat and Fluid Flow 18: 253–261, 1997

655 Avenue of the Americas, New York, NY 10010

0142-727X/97/$17.00
PII S0142-727X(96)00093-7

A velocity ratio of 0.6 was generated with initial turbulent boundary layers and was nominally two-dimensional (2-D). Velocity measurements were made on fine cross-plane grids across the wake region and at several streamwise locations using a two-component laser-Doppler anemometer (LDA).

The following describes the experimental setup, including the LDA for obtaining velocity measurements, and discussion of the results.

Flow configurations and instrumentation

The dividing mechanism concerned was made of 1.5 mm-thick fiberglass and had a blunt trailing edge. A schematic of the trailing-edge profiles are shown in Figure 1. All the lobed trailing edges have the same wavelength at 66 mm with an included divergence angle of 44° ($\varepsilon = 22°$). Each mixer spanned three full lobes (total 198 mm) in the test section, and the height to wavelength (h/λ) ratio was 0.5 (see Figure 1a).

The geometry shown in Figure 1b is a lobed forced mixer (LM) similar to that used by Yu et al. (1995). Strong streamwise vorticity can be shed at the trailing edge. To reproduce the forced mixer's trailing edge without the effects of the penetration angles, the convoluted plate (CP) in Figure 1c was constructed by extending the lobes in convoluted parallel sections. The extension is equal to one wavelength of the lobe trailing-edge profile. It has been shown previously that such geometry (Manning 1991) shed relatively little streamwise vorticity.

To illustrate the importance of streamwise vorticity further, a scalloped lobed mixer (SM) is designed (Figure 1d). Based on previous findings (Presz et al. 1995; Yu et al. 1996) that even stronger streamwise vorticity than the lobed mixer can be shed by eliminating part of the sidewall area at the penetration region of each lobe, a 25% sidewall area has been removed in the present case.

Wind tunnel

The wind tunnel used to obtain velocity measurements in the present investigation was similar to that used by Yu et al. (1995). In the present investigation, a mean speed of 8 m/s for the two coflowing streams had been used, corresponding to a Reynolds number of 3.624×10^4 (based on the nominal wavelength of the lobe at 66 mm). The free-stream turbulence level on either side of the lobed mixer is less than 1% of the local mean velocity. The temperature of the air was kept at 28° during the course of the experiment.

Laser-Doppler Anemometer

A four-beam, two-component, fiber-optic LDA manufactured by TSI Incorporated, with a 300 mW Argon air-cooled laser operating at a backward-scattered mode was used to measure the respective velocity components. A focusing lens of 400 mm provided a measuring probe volume of $0.091 \times 0.091 \times 1.8$ mm in the vertical direction and $0.12 \times 0.12 \times 2.1$ mm in the horizontal direction. The fiber-optic probe was mounted on an automated, three-dimensional (3-D) traversing system with an accuracy of ± 0.01 mm. Bragg shifting of up to 2 MHz (on each channel) was used for detecting directional ambiguity. The Doppler signals were collected by photomultipliers and processed by the burst spectrum analyzers (IFA 750). Fine water particles, within 5–10 μm, generated by a commercial vaporizer, were used to seed the flow. These were injected into the wind tunnel upstream of the settling chamber before the contraction section. Except for some regions immediately behind the trailing edge, data rate of 500–1000 Hz were normally obtainable. At each measuring point, the mean velocities, the rms of the velocity fluctuations, and the Reynolds shear stresses were determined from populations of more than 10,000 (on each channel) samples together with a coincidence window of 1 μs.

A careful appraisal of the errors associated with the LDA system was conducted. The sources of error were mainly from velocity biasing (Durao et al. 1979), velocity gradient broadening (Durst et al. 1981), accuracy of the signal processor, and the finite sampling size (Yanta and Smith 1973). Thus, accuracy of the measured velocity components (normalized by the bulk mean velocity of the two streams, U_r, 8 m/s) can be expected to be about 2% and that of the rms of the velocity fluctuations (normalized by U_r), and the Reynolds shear stresses (normalized by U_r^2), 5%, based upon a 95% confidence level.

The boundary layers measured on either side of the splitter plate at three wavelengths upstream of the trailing edge are given in Table 1.

Measurements of the three-orthogonal mean velocities (U, V, W), their corresponding rms fluctuations (u', v', w' but not presented), and Reynolds shear stresses ($\overline{u'v'}$, $\overline{u'w'}$ only but not presented) were acquired in the projected area corresponding to

Notation

C_1	normalized streamwise circulation, $\Gamma_s/U_r h \tan \varepsilon$
Re	Reynolds numbers, $U_r\lambda/\upsilon = 3.632 \times 10^4$
Re_Θ	Reynolds number based on the momentum thickness
h	lobe height, 66 mm
U_1, U_2	mean velocity of the top (low speed) and bottom (high speed) streams
U_r	reference mean velocity, $(U_1 + U_2)/2 = 8$ m/s
U, V, W	streamwise, horizontal, and vertical mean velocities
V_s	secondary mean velocity, $\sqrt{V^2 + W^2}$
x, y, z	streamwise, horizontal, and vertical directions

Greek

δ^*	displacement thickness, cm
ε	half of the included divergent angle of the penetration region, 22°
θ	shear layer entrainment momentum thickness, cm
λ	nominal lobe wavelength, 66 mm
υ	kinematic viscosity
Γ_s	streamwise circulation
H	boundary-layer shape factor, δ^*/Θ
Θ	momentum thickness, cm
Ω_x	streamwise mean vorticity, $= (\partial W/\partial y) - (\partial V/\partial z)$
Ω_y	normal mean vorticity (in the y-direction), $= (\partial U/\partial z) - (\partial W/\partial x)$
Ω_z	normal mean vorticity (in the z-direction), $= (\partial U/\partial y) - (\partial V/\partial x)$

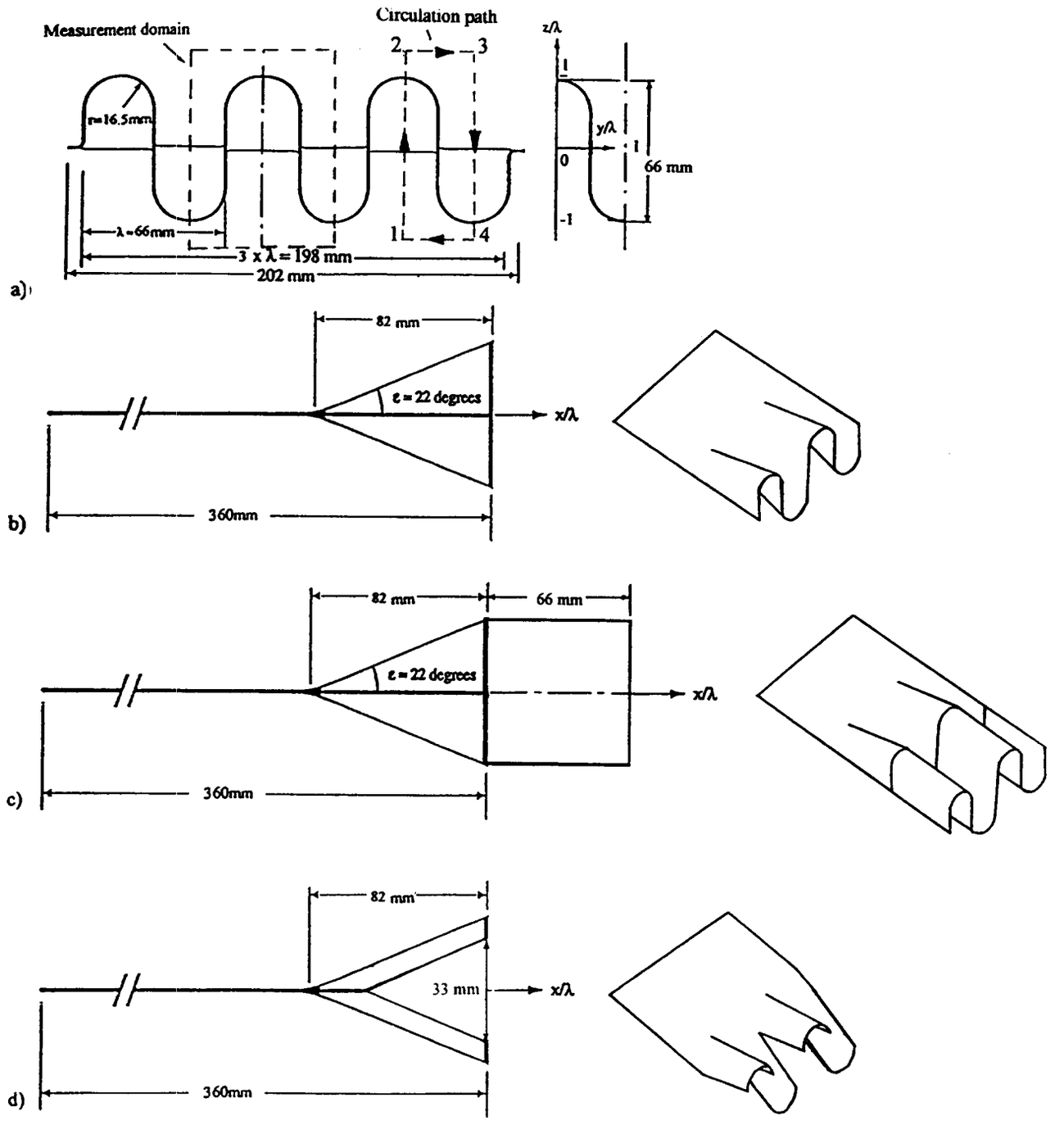

Figure 1 a) Dividing mechanism trailing-edge configuration and dimensions; b) lobed forced mixer; c) convoluted plate; d) scalloped forced mixer

Table 1 Boundary-layer parameters at three wavelengths upstream of the penetration region

Vel.ratio 0.6	δ, cm	Θ, cm	*H*	Re_Θ
Top stream	0.52	0.41	1.33	268
Bottom stream	0.38	0.31	1.31	161

the one lobe located close to the center of the test section and at downstream locations where $x/\lambda = 0.25, 0.5, 1, 1.5, 2, 3, 4$, and 5. At each station, there were about 1100 measuring points at each lobe. Different components of the vorticity (Ω_x, Ω_y, and Ω_z) were calculated based on a third-order polynomial fit to the U, V, and W measurements.

The average streamwise circulation at downstream locations was determined by obtaining line integration along a rectangular path that encompasses one-half the lobe wavelength (Barber

et al. 1988), as shown in Figure 1a. In nondimensional expression,

$$C_1 = \frac{\Gamma_s}{U_r h \tan \varepsilon} \tag{1}$$

where

$$\Gamma_s = \oint_{1-2} \mathbf{W}\,ds + \oint_{2-3} \mathbf{V}\,ds + \oint_{3-4} \mathbf{W}\,ds + \oint_{4-1} \mathbf{V}\,ds$$

Results and Discussion

Downstream development of streamwise and secondary mean velocities

The mean streamwise velocity contours (U/U_r) and the corresponding secondary mean velocity vectors (V_s/U_r) at four representative stations within the range of $x/\lambda = 0.5$–5.0 are presented in Figures 2–4 for the LM, SM, and CP cases, respectively. The formation of the streamwise vortices is obvious in the LM and SM cases immediately after the trailing edge at $x/\lambda = 0.5$ and Figures 2a and 3a. The center for each streamwise vortex appears at nearly the same locations for the two cases; i.e., at about the inflexion point of the projected lobe contour. The SM has the highest secondary flow velocities (maximum $0.65U_r$) compared with the LM (maximum $0.55U_r$) and CP (maximum $0.05U_r$) cases. As might be expected, no evidence of streamwise vortex formation can be found in the CP case (see Figure 4a). The distance between any two contour levels for the CP case, however, is relatively wider than the other two cases and can be attributed mainly to the presence of the extension, which facilitates the growth of the boundary layers along the sidewalls.

By $x/\lambda = 1.0$ and Figures 2b–3b, the streamwise vortices for both the LM and SM cases have been intensified, especially the SM case, causing the migration of the velocities, mainly from the low-speed side to the high-speed side. The pinched-off effects described by McCormick and Bennett (1994) can be observed clearly in the streamwise mean velocity contour distribution at this station for the LM and SM cases. Diffusion effects are found to be more obvious in the SM case than the LM case at the subsequent measured station $x/\lambda = 2.5$ (compare Figures 2c–3c). For the CP case and Figure 4c, the mean velocities are mainly diffused on every side of the projected lobe contour. Toward the end of the measurement domain and Figures 2d–3d, a fairly uniform distribution for the velocity contours has appeared along the y/λ directions; it appears earlier in the SM case at $x/\lambda = 4.0$ compared with the LM case at $x/\lambda = 5.0$. The corresponding strength for the secondary flow velocities is also much lower compared with that measured at the preceding stations for both the LM and SM cases. The dissipation for the streamwise vorticity is largely made up by the diffusion effects in the streamwise velocity field. Strength of the secondary flow velocities for the CP case at this location and Figure 4d is almost negligible compared with the other two cases, and maximum does not exceed $0.05U_r$ within the range of measurements.

Thus, the vortex development underwent a three-step process: the initial formation, the subsequent intensification, and the final dissipation. This is consistent with those observed in the visualization tests of Manning (1991).

Development of Mean Vorticity

Distortion of the mean velocities contours is obviously a direct result of the streamwise vorticity. The mean vorticity contours at four selective streamwise locations near the trailing edge for the SM case are presented in Figure 5. As may be expected from the mean velocity measurements, a single row of streamwise vortex is generated at each half-lobe immediately after the trailing edge at $x/\lambda = 0.5$ and Figure 5a. The peak mean streamwise vorticity maintains nearly the same strength from about $x/\lambda = 1.0$–1.5 (see Figures 5b–5c) and is clearly decreasing rapidly with downstream distance after $x/\lambda = 2.0$ and Figure 5d. It should be noted that the reorientation of the normal vorticity as the flow developed downstream did not seem to affect the location of the streamwise vortex. Because the vortex spacing within a lobe is maintained at the same distance within the range of measurements, it seems that the decrease of the vortex strength is the direct result of the viscous dissipation.

The streamwise evolution of the average circulation per vortical structure is presented in Figure 6. The average circulation for each vortex is evaluated using Equation 1 and is found to be the highest for the SM case near the trailing edge. The strength of the streamwise circulation shed at the trailing edge of the SM case is equivalent to a nonscalloped LM case of larger penetration angle at 28°. The CP case near the trailing edge is much lower than the SM and LM cases, but the rates of reduction are somewhat different so that they only become comparable after $x/\lambda = 4.0$. By $x/\lambda = 5.0$, the circulation for all cases reduce to a negligible level.

Development of momentum entrainment thickness

The momentum entrainment thickness that defines the amoumt of fluid being entrained into the wake by the streamwise vorticity can be calculated by the following expression and is shown in Figure 7.

$$\theta = \int (U - U_2)(U_1 - U)/\Delta U r^2 \, dz \tag{2}$$

The increasing rate is very rapid from the trailing edge to $x/\lambda = 2.0$ for both the SM and LM cases, and beyond $x/\lambda = 2.0$, the growth rate reduces and becomes lower than that of CP case. The increasing rate of the CP case is obviously lower than the other two cases. The results are not unexpected, because in the absence of the streamwise vorticity, the entrainment for the CP case would rely solely on the 2-D roll-up of the normal vorticity that is obviously lower than the cases with streamwise vorticity. The comparison highlights the fact that the presence of the streamwise vorticity greatly enhances the initial entrainment growth rate. When the streamwise vorticity is dissipated, the corresponding entrainment growth rate becomes slower than that of the CP case, which has an undistributed roll-up of the normal vorticity from the trailing edge. The results obtained here are again consistent with those observed in visualization tests (Manning 1991).

Conclusion

The mixing characteristics of two-stream mixing flows have been investigated using a two-component LDA. The trailing-edge profiles for the dividing mechanism include an LM, an SM, and a convoluted plate. Scalloping effect was achieved by eliminating up to 25% of the sidewall area at the penetration region of each lobe. The convoluted plate was constructed by extending the lobes in convoluted parallel sections by one wavelength downstream. For the three cases considered, trailing-edge wavelength and the penetration angle were maintained the same.

The results indicated that the SM has generated the highest streamwise vorticity at the trailing edge than the LM and convoluted plate. The subsequent decay rate is also found to be more rapid for the SM than the other two cases. For the case of the

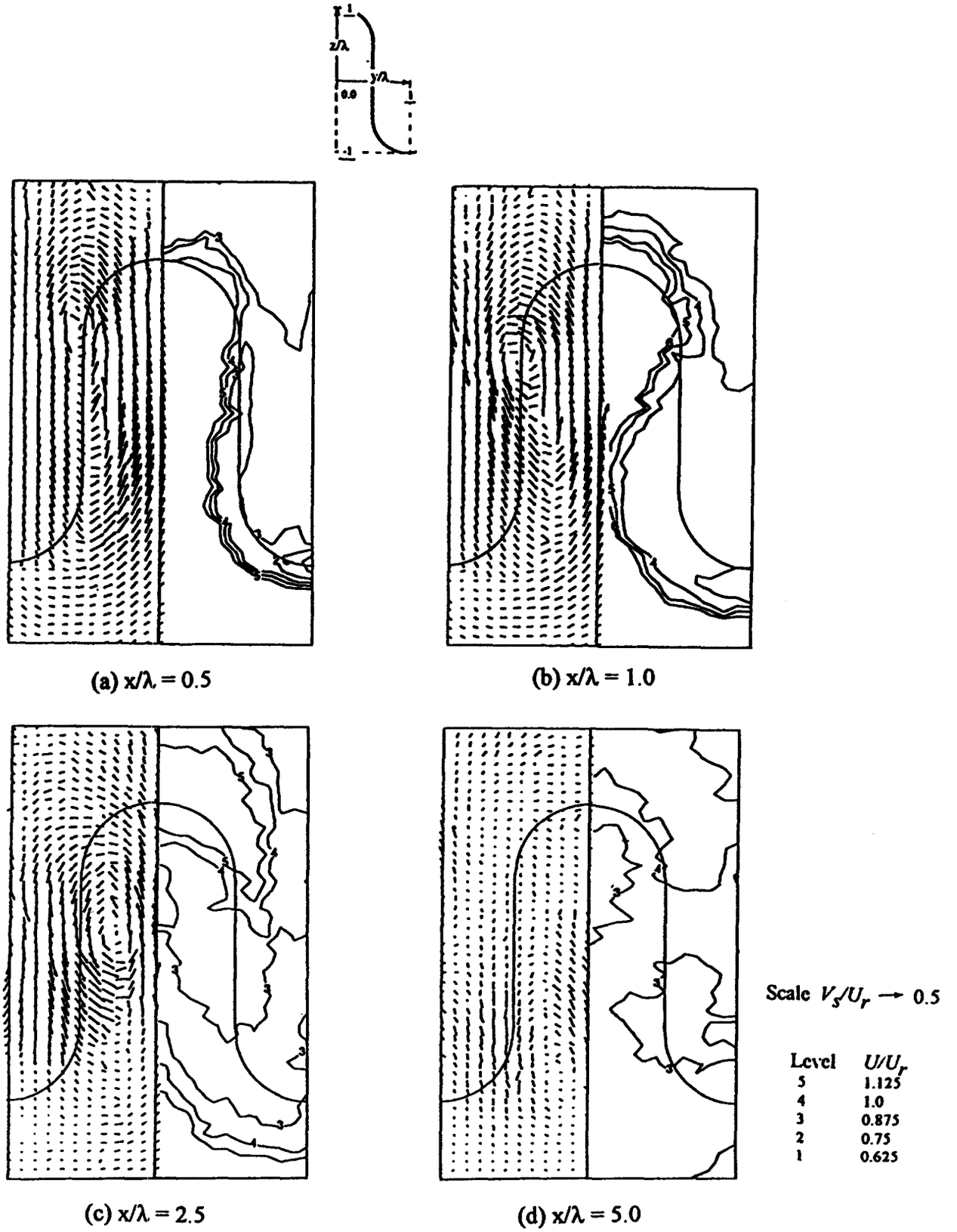

Figure 2 Contours of the normalized streamwise mean velocity (U/U_r) and the corresponding secondary flow velocity vectors (V_s/U_r) at successive downstream stations of the lobed forced mixer trailing edge

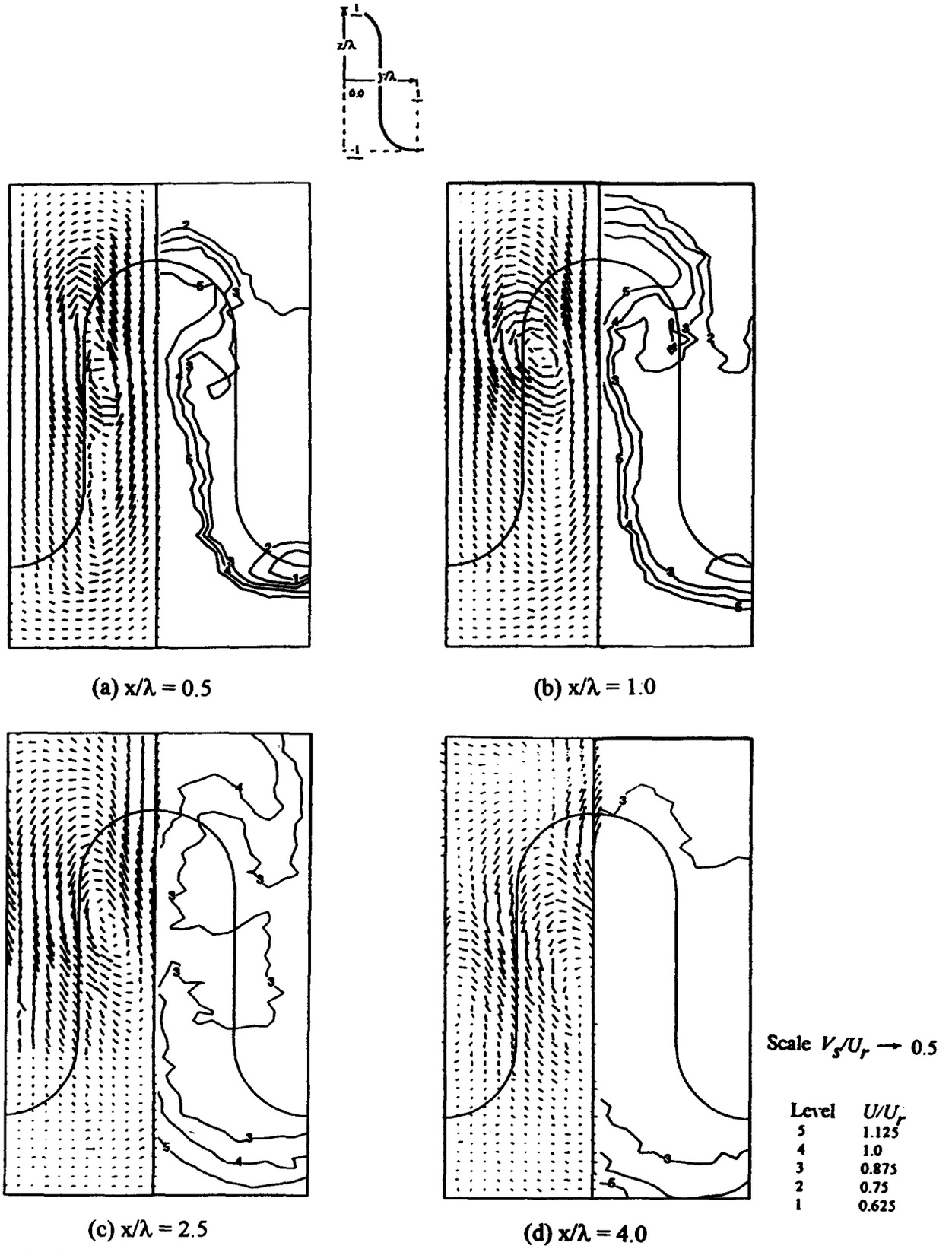

Figure 3 Contours of the normalized streamwise mean velocity (U/U_r) and the corresponding secondary flow velocity vectors (V_s/U_r) at successive downstream stations of the scalloped mixer trailing edge

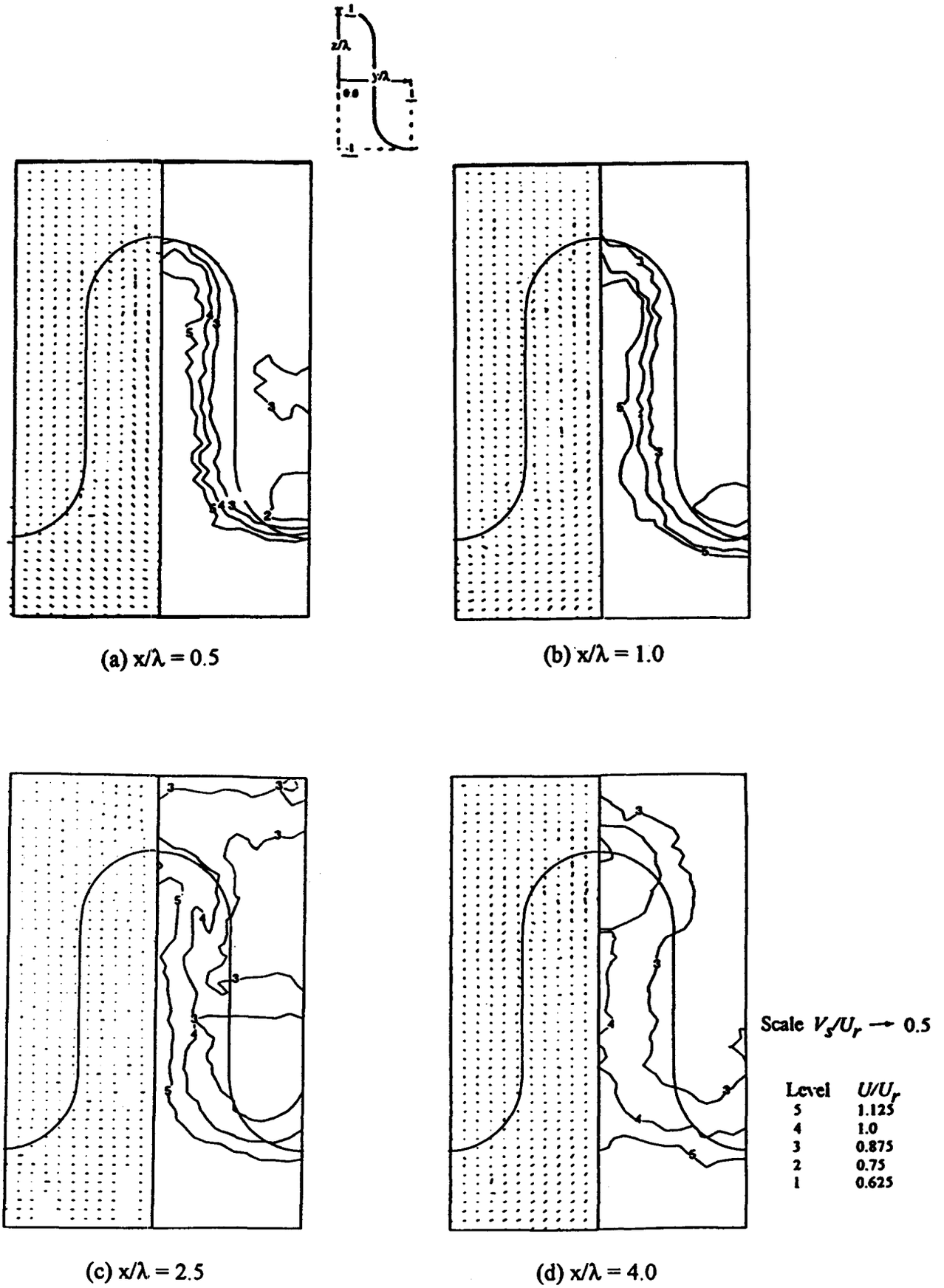

Figure 4 Contour of the normalized streamwise mean velocity (U/U_r) and the corresponding secondary flow velocity vector (V_s/U_r) at successive downstream stations of the convoluted plate trailing edge

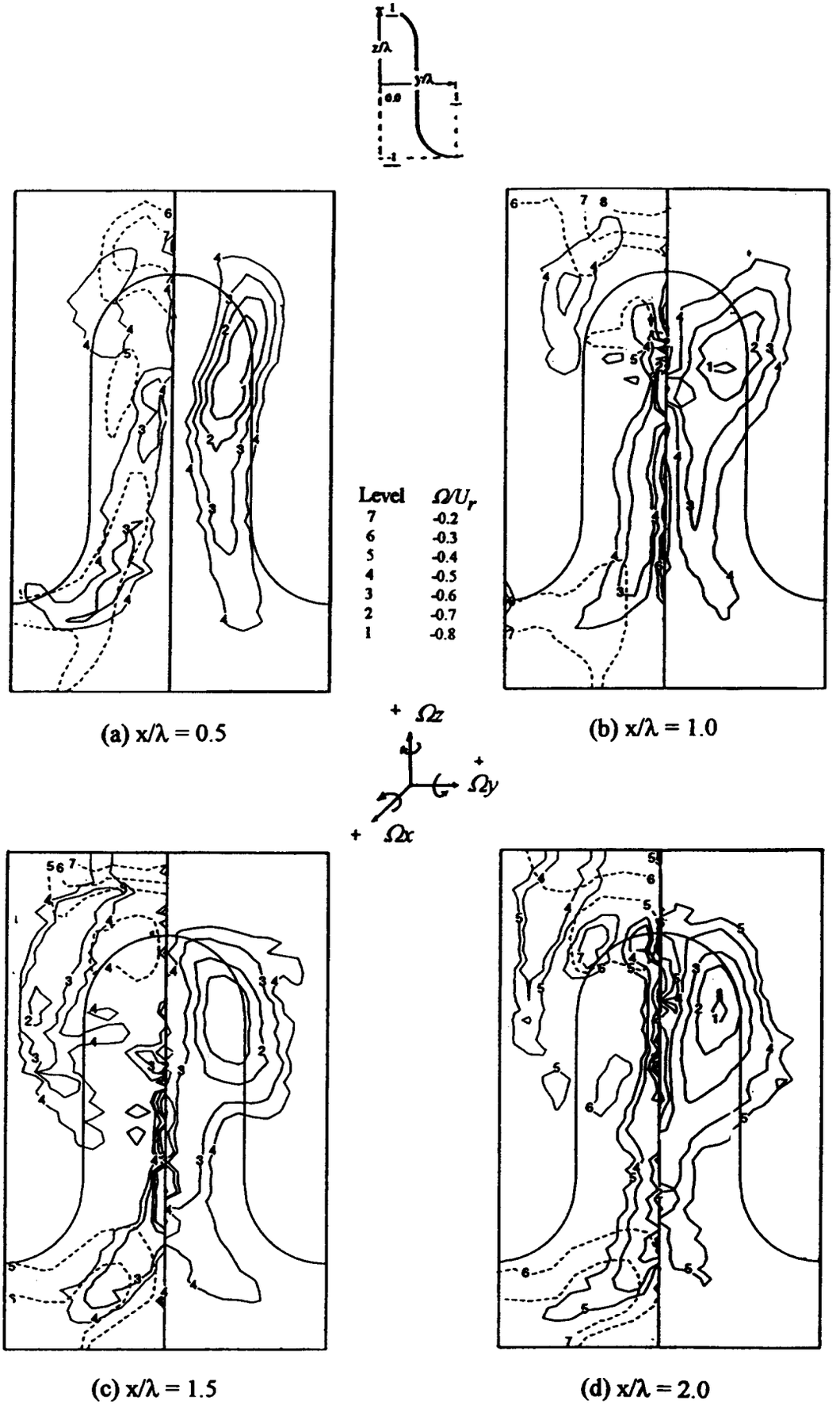

Figure 5 Contours of the normalized velocities at successive downstream stations of the scalloped mixer trailing edge (left side ----Ωy —Ωz, right side —Ωx)

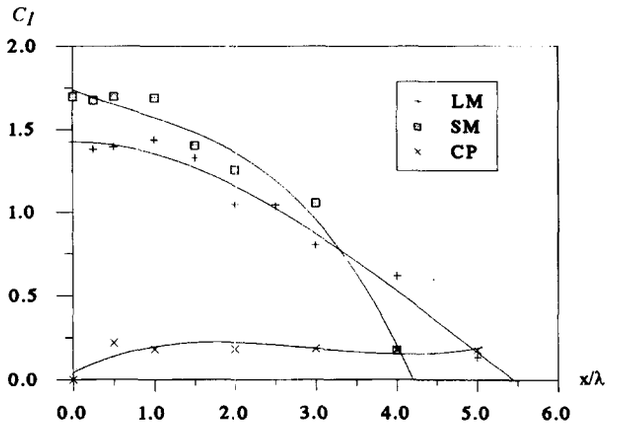

Figure 6 Variation of average streamwise circulation with downstream distance (trailing-edge values were obtained from the theory of Barber et al. 1988)

convoluted plate, very little streamwise vorticity is shed at the downstream wake.

For the lobed and the scalloped mixers, the streamwise vortex development for the two cases underwent a three-step process by which it was formed, intensified, and quickly dissipated. Thus, the present measurements are consistent with those found in visualization tests (Manning 1991). The interfacial area for the scalloped mixer is actually lesser than that of the LM. Thus, the SM should be a more efficient mixing device, because it not only can shed a higher strength of streamwise vorticity; it can also provide a relatively lower induced drag.

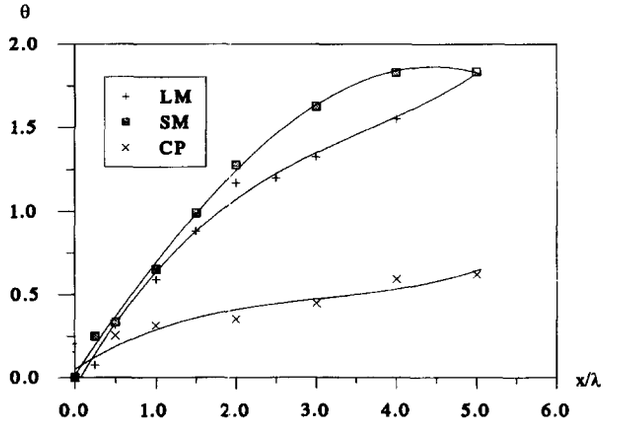

Figure 7 Variation of momentum thickness with downstream distance

As a result of the streamwise vorticity, the shear-layer entrainment growth rates are very rapid for the SM and LM from the trailing edge to about $x/\lambda = 2.0$. At the region where the streamwise vorticity is almost dissipated, the growth rates reduce rapidly and become lower than those of the convoluted plate case. The shear layer growth for the convoluted plate, which has little influence on streamwise vorticity, depends solely on the roll-up of the normal vorticity and is therefore much lower than cases with streamwise vorticity.

Acknowledgments

Financial support for this project from the Academic Research Fund and a graduate scholarship for T. H. Yip from the School of Mechanical and Production Engineering are gratefully acknowledged.

References

Bell, J. H. and Mehta, R. D. 1992. Measurements of the streamwise vortical structures in a plane mixing layer. *J. Fluid Mech.*, **239**, 213–248

Bell, J. H. and Mehta, R. D. 1993. Effects of imposed spanwise perturbations on plane mixing-layer structure. *J. Fluid Mech.*, **257**, 33–63

Barber, T., Paterson, R. W., and Skebe, S. A. 1988. Turbofan forced mixer lobe flow modeling, Vol. 1: experimental and analytical assessment. NASA CR4147

Durao, D. F. G., Laker, J., and Whitelaw, J. H. 1979. Bias effects in laser-Doppler anemometry. *J. Phys. E: Sci. Instrum.*, **13** 442

Durst, F., Melling, A., and Whitelaw, J. H. 1981. *Principles and Practice of Laser-Doppler Anemometry*, Academic Press, London

Eckerle, W. A., Sheibani, H., and Awad, J. 1992. Experimental measurement of the vortex development downstream of a lobed forced mixer. *ASME J. Eng. Gas Turbines Power*, **114**, 63–71

Manning, T. A. 1991. Experimental studies of mixing flows with streamwise vorticity, M.S. thesis, Massachusetts Institute of Technology, Cambridge, Massachusetts, USA

McCormick, D. C. and Bennett, J. C. Jr. 1994. Vortical and turbulent structure of a lobed forced mixer free-shear layer. *AIAA J.*, **32**, 1852–1859

Presz, W. M., Reynolds, G., and McCormick, D. 1994. Thrust augmentation using mixer–ejector-diffuser systems. AIAA paper 94-0020

Yu, S. C. M., Yeo, J. H., and Teh, J. K. L. 1995. Velocity measurements downstream of lobed forced mixers with different convoluted trailing edge configurations. *J. Propulsion Power*, **13**, 87–97

Yu, S. C. M., Xu, X. G., and Yip, T. H. 1996a. Effects of initial boundary-layer thicknesses to the lobed forced mixer trailing streamwise vorticity. *J. Propulsion Power*, **14**, 440–442

Yu, S. C. M., Yip, T. H., and Liu, C. Y. 1997. The mixing characteristics of forced mixers with scalloped lobes. *J. Propulsion Power*, **15**, 1–7

Yanta, W. J. and Smith, R. A. 1973. Measurements of turbulence